UNIVERSITY OF WATERLOO
Faculty of Science

Phys 375 Individual Report

Phys 375 - University of Waterloo
Waterloo, Ontario

prepared by

Joshua Lau
3B Physics and Astronomy
ID 20630767
April 17, 2019

Table of Contents

List of Figures

List of Tables

1.0 Algorithm

1.1 Runge Kutta Method

The main bulk of work in this project is trying to solve stellar struction differential equations. To tackle this task of solving coupled ODE's our group decided to use 4th order Runge Kutta Method (RK4). The RK4 is a numerical analysis algorithm for finding solutions to ODE's. The method of RK4 is as follows; for a given differential equation:

$$\frac{dy(x)}{dx} = f(y(x), x) \tag{1}$$

If we know the initial conditions $y(0) = y_0$. The RK4 method approximates the value of y_{n+1} with the following coefficients:

$$\begin{aligned} k_1 &= hf(y_n, x) \\ k_2 &= hf(y_n + \frac{k_1}{2}, x_n + \frac{h}{2}) \\ k_3 &= hf(y_n + \frac{k_2}{2}, x_n + \frac{h}{2}) \\ k_4 &= hf(y_n + k_3, x_n + h) \\ y_{n+1} &= y_n + \frac{1}{6}(k_1 + k_2 + k_3 + k_4) \end{aligned}$$

Where h is the step height $h = x_{n+1} - x_n$. Initially at x_0 the first coefficients k_1 is the slope at the beginning of x-value step. Next k_2 is the slope at the midpoint of the interval using the previous k_1 value. Furthermore k_3 is the slope of the at the midpoint but based on k_2 value. Finally k_4 is the slope at the endpoint. This process keeps on looping until the surface conditions of our stellar equations are satisfied. Our surface conditions are based on $\Delta\tau < 0.001$ and also physical limits on mass and radius. We mainly decided to use RK4 as we felt that it should be sufficiently accurate enough to give us correct values of temperature, density, luminosity, and so on. With the RK4 method we get that truncation error on the order of $O(h^5)$ and accumulated error on the order $O(h^4)$

1.2 Bisection Method

Once the surface condition is satisfied in the RKsolver function the program than moves onto the bisection method to find the roots of a trial function. Using the course notes the trial function is defined [1]:

$$f(\rho_c) = \frac{L_* - 4\pi\sigma R_*^2 T_*^4}{\sqrt{4\pi\sigma R_*^2 T_*^4}} \tag{2}$$

Our bisection method follows the standard procedure of chopping up the intervals by half every loop and the condition $f(a)f(b) < 0$. However one computation decision we made is we implemented a "step down" approach. Where instead of starting at an interval $[a_0, b_0]$ our bisection begins at the top bound of ρ_c and work it's way down until a solution is found. We implemented this approach since stepping down from the top bound of ρ_c saves a lot more than as oppose to the standard method of beginning at an interval $[a_0, b_0]$. Finally the whole process of our code can be summarized in the following flowchart:

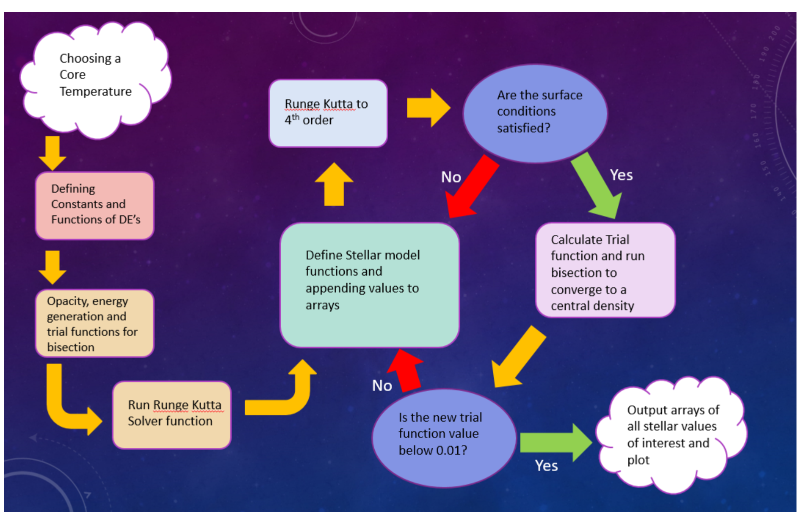

Figure 1: Flowchart of our Stellar Model Code

2.0 Main Sequence

Below is the main sequence we were able to produce from our code. The surface temperature runs from around 1500K to 7500K and consist of 32 stars. Unfortunately due to the time constraints we were not able to produce stars with surface temperature greater than 7500k.

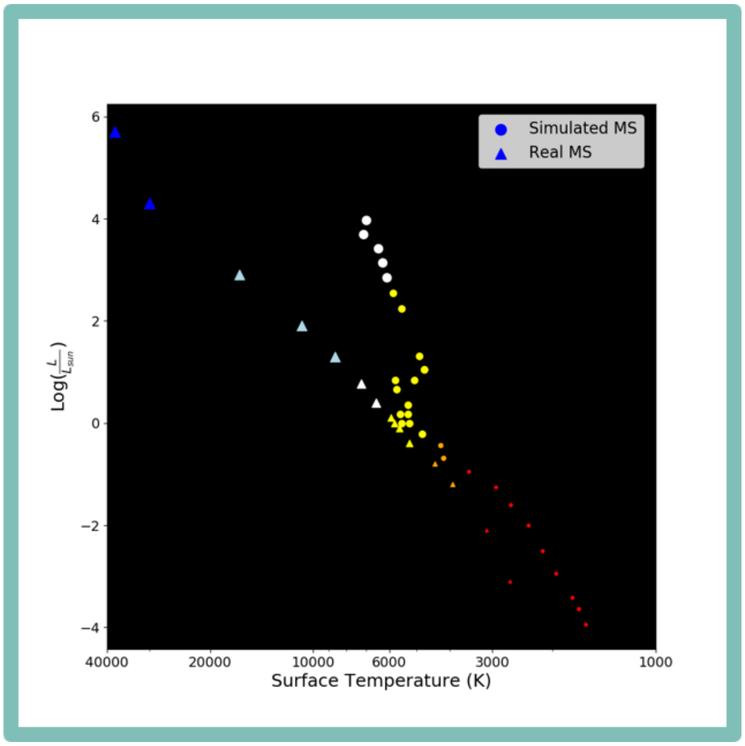

Figure 2: Our Main Sequence

One key comment that must be made is that near the 6000K mark there is a cluster of stars then a rapid increase of the stars luminosity, this is mainly due to the fact that mid way through producing the main sequence we modified the code to make it more efficient and might have ended up changing the values of stars past 6000k. However we were able to capture the expected trend as surface temperature increases the luminosity did as well. Thus our main sequence agrees with the theory.

Note in figure (2) of our main sequence we also plotted real star values to compare with our model. These sample points were taken from wikipedia's page of main sequence [3].

Next we are able to produce our L/L_{sun} vs M/M_{sun} and R/R_{sun} vs M/M_{sun} for our 32 stars. Within both graphs we can also plot the empirical results of page 330 from the textbook "Foundations of Astrophysics" [2]. The Empirical conditions for radius and luminosity are as follows:

$$R/R_{sun} = 1.06(M/M_{sun})^{0.945} \qquad M < 1.66M_{sun}$$

$$R/R_{sun} = 1.33(M/M_{sun})^{0.555} \qquad M > 1.66M_{sun}$$

$$L/L_{sun} = 0.35(M/M_{sun})^{1.62} \qquad M < 0.7M_{sun}$$

$$L/L_{sun} = 1.02(M/M_{sun})^{3.92} \qquad M > 0.7M_{sun}$$

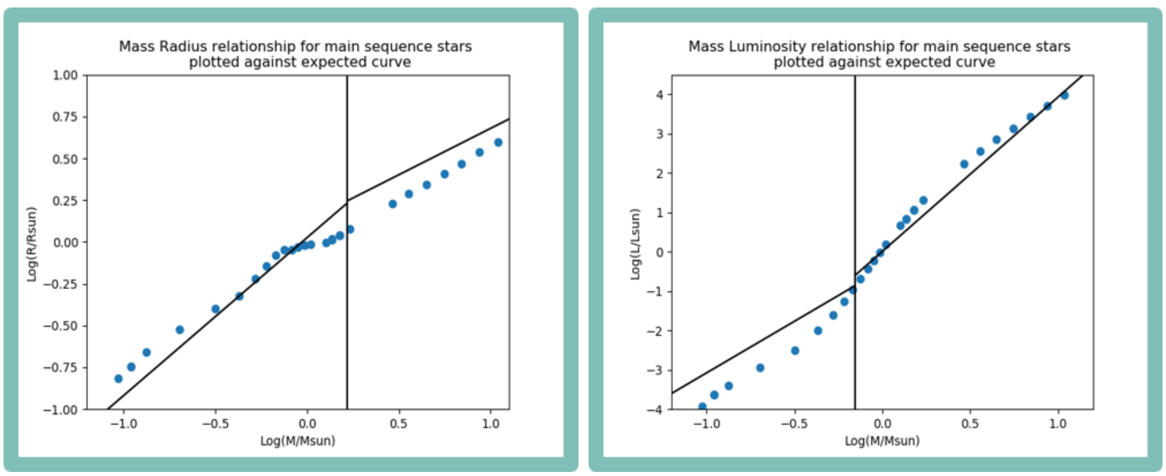

Figure 3: Normalized Luminosity and Radius plots versus Mass

3.0 Stellar Models

From the our code we generated two stars, one above and below the mass of the sun. The table below gives the stellar values such as temperature, density, luminosity and so on:

	Small Star	Large Star
Central Density ($\frac{kg}{m^3}$)	77062	18276
Central Temperature (K)	9x10^6	2.5x10^7
Surface Temperature (K)	3363	5413
Mass (M_{sun})	0.673	4.47
Luminosity (L_{sun})	0.111	703
Radius (R_{sun})	0.799	2.1

Table 1: Stellar values of two stars produced from our code

Next for each star there are 5 associated plots below: normalized M, ρ, T, L vs radius, Normalized Pressure and its components vs radius, $\frac{dlogP}{dlogT}$ vs radius, κ vs radius, and $\frac{dL}{dr}$ vs radius. The left column of plots is the smaller star with mass $0.673M_{sun}$ and the right column is the star with mass $2M_{sun}$

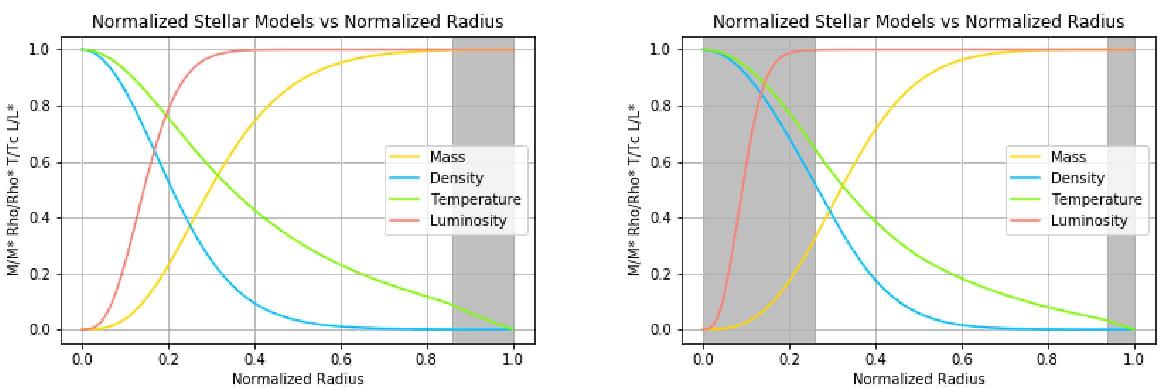

Figure 4: Normalized Stellar Structure Plots: Luminosity, Density, Temperature, Mass versus Radius

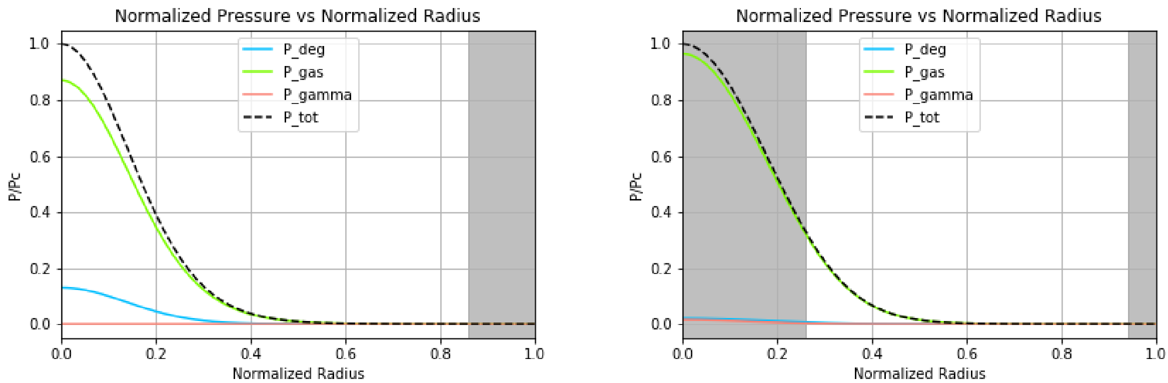

Figure 5: Normalized Pressure versus Normalized Radius

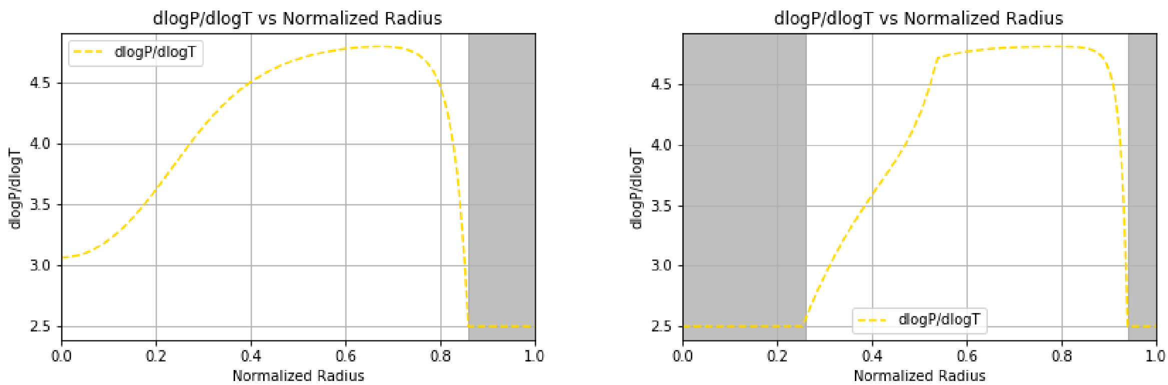

Figure 6: dlogP/dlogT versus Normalized Radius

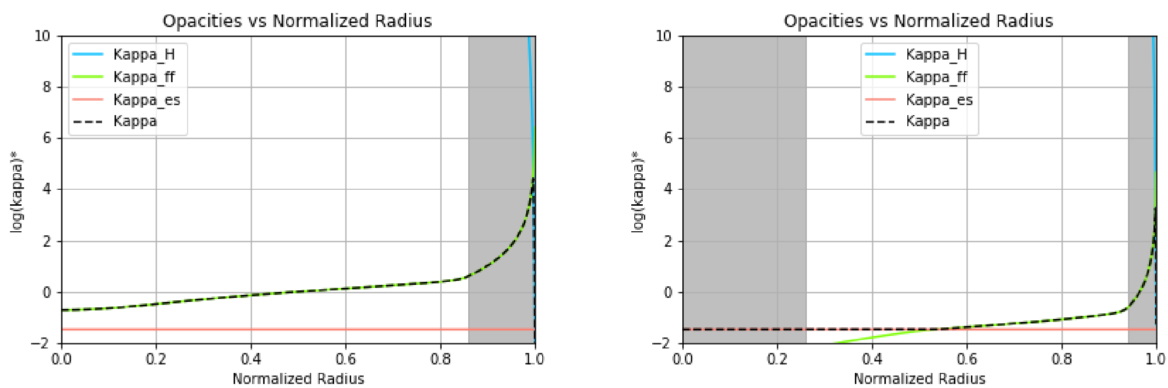

Figure 7: $\log(\kappa)$ vs Normalized Radius

When these two stars with mass $0.673M_{sun}$ and $4.47M_{sun}$ are compared there are two key features that needs to be discussed. From figure 6 we see that the larger star $4.47M_{sun}$ has

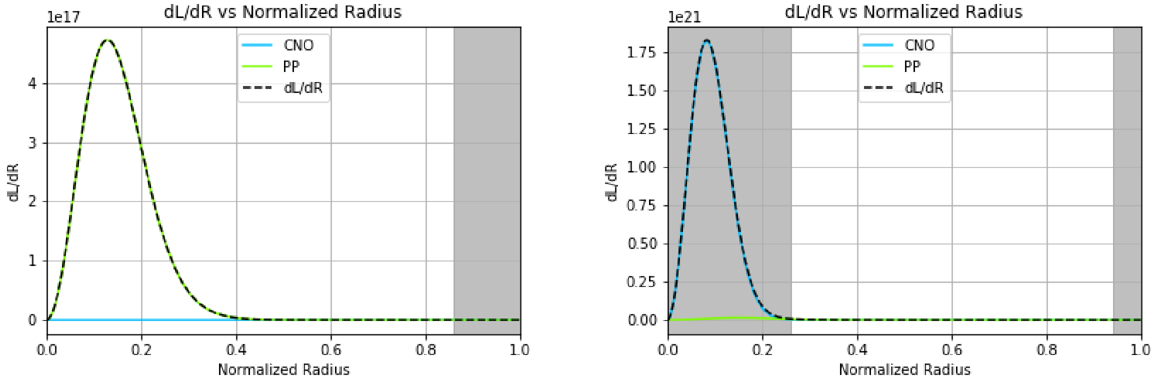

Figure 8: dL/dr versus Normalized Radius

two convection zones while the smaller star has only 1. This arises due to the condition of convection given by [1]:

$$\frac{dT}{dr} = -min[\frac{3\kappa\rho L}{16\pi acT^3r^2}, (1 - \frac{1}{\gamma})\frac{TGM\rho}{Pr^2}] \tag{3}$$

Where convection and radiative diffusion is given by [1]:

$$convection = (1 - \frac{1}{\gamma})\frac{TGM\rho}{Pr^2} \tag{4}$$

$$RadDiff = \frac{3\kappa\rho L}{16\pi acT^3r^2} \tag{5}$$

From figure (6) we see that the larger star's first convection zones begins in the center and reaches up to about $0.26R_{star}$ and the second convection zones goes from $0.94R_{star}$ to the surface. As oppose to the smaller star where the convection zone goes from 0.86 to the surface. The reason for the larger star having a convection zone in the core is due to the pressure term P in the denominator of equation (4). With the pressure being incredible large at the core of the sun this makes the convection term have a "flatter" slope than the radiative diffusion. But once the pressure begins to decrease as the radius increases the radiative diffusion begins to have the flatter slope.

Next from figure 8 we notice that the dominant energy generation between the two stars are different. For the smaller star the rates is governed by PP chain while for the larger is the CNO cycle. If we look at the two energy generation rates [1]:

$$\epsilon_{pp} = 1.07x10^{-7}\rho_5 X^2 T_6^4 \tag{6}$$

$$\epsilon_{CNO} = 8.24x10^{-26}\rho_5 X X_{CNO} T_6^{19.9} \tag{7}$$

An important feature of the CNO cycle is that it only stars at temperature of around 1.5x10^7 [2]. As a result the smaller star with core temperature of only 9x10^6 isn't hot enough to begin the CNO cycle thus it's energy generation is solely dependant on pp chain. However for the hotter larger star with core temperature 2.5x10^7 it is sufficiently hot enough to begin CNO cycle. From equation (6) and (7) we see that CNO cycle is also higher dependant on the temperature with $T^{19.9}$ vs pp chain's T^4 thus at high temperature CNO will completely dominate the energy generation rates.

Lastly opacities will be looked at in figure (7). The equations of opacities is given by [1]:

$$\kappa(\rho, T) = [\frac{1}{\kappa_{H-}} + \frac{1}{max(\kappa_{es}, \kappa_{ff}}]^{-1} \tag{8}$$

Where the opacity terms are [1]:

$$\kappa_{ff} = 1.0x10^{24}(Z + 0.0001)\rho_3^{0.7}T^{-3.5} \tag{9}$$

$$\kappa_{H-} = 2.5x10^{-32}(\frac{Z}{.02})\rho_3^{0.5}T^9 \tag{10}$$

$$\kappa_{es} = 0.02(1 + X) \tag{11}$$

First the contribution of κ_{es} for both graphs is the same since it doesn't depend on the density but on X only. For both stars the metallicity is the same. For the smaller star see that it is mostly dominated by κ_{ff} up until the point before the surface where κ_{H-} pulls the opacity down to 0. For the large star however we see that initially the opacity is determined by κ_{es} up until about 0.6 of the radius. This most likely due to the very small prefactors in the equation for κ_{H-} and κ_{ff}. For κ_{ff} since it has a $T^{-3.5}$ dependence the contribution of isn't enough until the temperature is sufficiently low enough where κ_{ff} takes over the κ_{es}. But near the surface both stars behave the same where κ_{ff} drops off and κ_{H-} takes over and brings the overally opacity to 0.

4.0 References

[1] Broderick, Avery .PHY 375 Final Project . Waterloo(ON): University of Waterloo

[2] Ryden, B.S. & Peterson, B.M.(2010). Foundations of Astrophysics. San Francisco: Addison-Wesley

[3] Wikipedia contributors. Main sequence [Internet]. Wikipedia, The Free Encyclopedia; 2019 Mar 30, 10:55 UTC [cited 2019 Apr 17]. Available from: https://en.wikipedia.org/wiki/Main_sequence.